PERGAMON

Applied Radiation and Isotopes 55 (2001) 707–713

Applied Radiation and Isotopes

www.elsevier.com/locate/apradiso

Bronchial dosimeter for radon progeny

T.T.K. Cheung[a], K.N. Yu[a,*], D. Nikezic[a,b]

[a] *Department of Physics and Materials Science, City University of Hong Kong, Tat Chee Avenue, Kowloon Tong, Hong Kong*
[b] *University of Kragujevac, Faculty of Sciences, 34000 Kragujevac, Yugoslavia*

Received 19 December 2000; received in revised form 7 May 2001; accepted 4 June 2001

Abstract

A true bronchial dosimeter has been designed, consisting of four 400-mesh wire screens and a filter paper. With a face velocity of 3.3 cm s^{-1} for home exposure and 4.6 cm s^{-1} for mine exposure, the deposition pattern on the wire screens were found to satisfactorily match the variation of the dose conversion factor (in units of mSv WL M^{-1}) with the size of radon progeny from 1 to 1000 nm. In this way, the bronchial dosimeter directly gives bronchial dose from the alpha counts recorded on the wire-screens and the filter paper. Calculations of the dose conversion coefficient (DCC) using the proposed bronchial dosimeter and the lung dosimetric model were performed for typical aerosol characteristics. Values obtained from the bronchial dosimeter yielded overestimates of the DCC by 11.1% and 2.4% for typical home and mine conditions, respectively. © 2001 Published by Elsevier Science Ltd.

Keywords: Dosimetry; Dose; Lung model; Radiation

1. Introduction

Over the past several decades considerable attention was focussed on the potential hazard from exposure of the general population to radon (^{222}Rn) and its progeny, both in the work place and at home. It is now established that the inhalation of airborne short-lived radon progeny in the indoor and outdoor environment yields the greatest amount of natural radiation exposure to the public. The major health concern comes from the deposition of radon progeny on the epithelial cells of the bronchial airways (James, 1984). To assess the corresponding bronchial dose, the use of dosimetric lung models is necessary. In this method, information on several important parameters such as the unattached fraction (f_p), the potential alpha energy concentration (PAEC) of radon progeny and the equilibrium factor (F) are required.

Measurements of the unattached fraction based on wire screen methods have only been partially successful (Ramamurthi and Hopke, 1989). In particular, the collection efficiency versus particle diameter characteristics of wire screens has not permitted a distinct separation of the unattached and attached fractions. Hopke et al. (1990) suggested that the deposition characteristics of short-lived progeny in the nasal and tracheobronchial (T-B) regions be simulated and the deposited activity measured directly. They provided a detailed conceptualization of such a measurement system and proposed the use of multiple wire screens to simulate the collected characteristics of the nasal and T-B regions. In accordance with such specification, Oberstedt and Vanmarcke (1995) built and calibrated a measurement system called the bronchial dosimeter consisting of three sampling heads, removing difficulties in measuring the activity median diameter (AMD) and the unattached fraction. However, this bronchial dosimeter only gave the fractional deposition of PAEC in the T-B region. For determining the bronchial dose, further assumptions and calculations were needed.

As such, it is of interest to find ways to obtain the bronchial dose directly. This paper outlines the conceptual procedures for developing such a dosimeter based on the collection efficiencies of wire screens.

*Corresponding author. Tel.: +852-2788-7812; fax: +852-2788-7830.

E-mail address: peter.yu@cityu.edu.hk (K.N. Yu).

0969-8043/01/$ - see front matter © 2001 Published by Elsevier Science Ltd.
PII: S0969-8043(01)00117-8

2. Methodology

2.1. Dosimetric lung model

The traditional approach to calculation of the radiation dose from inhalation of airborne short-lived radon progeny is dosimetric modeling of the respiratory tract. For modeling deposition and movement of the inhaled aerosols, the descriptive features of the T-B tree must first be formalized into distinct quantities which can appear in mathematical functions. In the present work the ICRP lung morphometric model (ICRP, 1994) has been employed, incorporating a dichotomous branching scheme in a symmetric tree in which daughter generations branch with relatively little irregularity. Each generation of the lung divides its passageways into two identical subpassages, which in turn evolve into the next generation. A typical airway is represented by a cylindrical tube of appropriate wall thickness with fixed dimensions. The dimensions of the airway branches gradually change as they penetrate deeper into the lung. In general, the average diameter and length of the tubes decrease with increasing order of generation. The T-B tree is considered to comprise bronchial (BB) and bronchiolar (bb) regions. In addition, the sensitive targets for respiratory tract cancers that are likely to result from radiation exposure need to be identified. The nuclei of secretory and basal cells have been considered to be the sensitive targets in the BB region, while only secretory cells have been considered in the bb region. Equal radio-sensitivities were assumed for these two types of cells.

Radiation doses to tissues and cells of the respiratory tract are functions of the air flow rate through the lung passages. Since considerable variability exists in the breathing characteristics and respiratory parameters, average values for normal and healthy people have been used. To predict radiation doses for different types of population groups, different breathing rates need to be matched to particular situations. Reference values of breathing rates for mine workers (Mines) and members of the public (Homes) have been chosen to be 1.2 and $0.78\,m^3\,h^{-1}$, respectively (Zock et al., 1996).

Estimate of the fractions of inhaled progeny deposited in each anatomical region is the next step in this process. Several processes contribute to the aerosol deposition. The most important of the mechanisms include Brownian diffusion, inertial impaction and sedimentation. The relative contributions from these processes depend upon the size distribution of the inhaled aerosols, the model being required to estimate regional deposition for a wide range of particle sizes. To provide a straightforward model, an empirical mathematical approach was applied to describe the regional deposition in the extrathoracic and thoracic airways (ICRP, 1994; James et al., 1991; NRC, 1991).

The inhalation process continuously deposits radon progeny in different branching generations of the lung. The deposited progeny are assumed to distribute uniformly on the surfaces, and are cleared by mucociliary transport or absorption into blood with an assumed transit time of 10 h for the slow transfer process (Zock et al., 1996).

To sum up the regional doses for the respiratory tract, they must be adjusted for their relative radiation sensitivities. The total lung dose was calculated by introducing equally weighted apportionment factors between BB, bb and alveolar-interstitial (AI) regions as 0.333 : 0.333 : 0.333. The weighting factor of 0.12 specified for lungs was also applied to the total dose calculated for the thoracic region, together with the quality factor of 20 for alpha particles, to obtain the effective dose. Dividing by the exposure, the dose conversion factor (DCF) in unit of $mSv\,WL\,M^{-1}$ was obtained. Based on the definition of an occupational working month as 170 h and making provision for an occupancy factor, a factor for effective dose rate (EDF) having the units of $mSv(s\,WL)^{-1}$ or $mSv(y\,WL)^{-1}$ could be derived from the DCF. Once the PAEC is known for a particular environment, the corresponding EDF can be determined. To fit the DCF distribution (with progeny size), the EDF distribution was normalized using a normalizing factor (n-factor) to obtain the distribution of normalized effective dose rate (NDF). From the knowledge of or assuming the progeny size distribution of an environment of interest, the effective dose per unit exposure to radon progeny (dose conversion coefficient, DCC) can be computed for that situation.

2.2. Fitting the DCF distribution

The particle-size dependent diffusion coefficient is commonly estimated by the Einstein equation modified with the Cunningham correction factor. Based on the fan model filtration theory (Cheng and Yeh, 1980; Cheng et al., 1980), a semi-empirical equation of particle penetration through wire screens was employed. The penetration for a wire screen, with solid volume fraction α, wire thickness w and diameter d_f, is given by

$$P = \exp\left(-\frac{4\alpha w}{\pi(1-\alpha)\,d_f}\varepsilon\right), \tag{1}$$

where ε is the single fiber collection efficiency expressed as a sum of the efficiencies for several deposition processes including diffusion ε_d, interception ε_{in}, impaction ε_{im}, and diffusional interception ε_{id}. In fact, the diffusion process dominates the overall collection efficiency for particle diameters below 100 nm. The interception and impaction processes become significant after a few μm. The efficiency for diffusional interception is insignificant compared to that for diffusion of particle

diameters up to beyond 1 μm. The mathematical representations for the four deposition efficiencies can be found elsewhere (Porstendörfer, 1996). The wire screen collection efficiency is simply equal to (1–P). Using N wire screens with the same wire factor WF in series, the exponent in Eq. (1) should be multiplied by N to obtain the gross penetration. The value of WF characterizes a particular wire screen, through the use of the representation

$$\mathrm{WF}[\mathrm{cm}^{-2/3}] = \frac{\alpha w}{(1-\alpha)d_f^{5/3}}, \tag{2}$$

and by incorporating the sampling face velocity U, the wire-velocity parameter KVF is defined as

$$\mathrm{KVF}[\mathrm{cm}^2/\mathrm{s}] = \frac{U}{[\mathrm{WF}]^{1.5}} \tag{3}$$

Each wire screen has its own WF. All the collection efficiencies, with the exception of that for interception, change according to U. Hence, varying U represents one way to shift the NDF distribution curve with progeny particle diameter (Fig. 1). The NDF curve can also be changed by using different combinations of wire screens (Fig. 2). For large particle sizes ranging from around tens of nm to 1 μm, corresponding to the attached mode of radon progeny, both techniques have failed to produce satisfactory fits to the NDF response. A factor (called k-factor in this paper), employing the residual efficiency of a filter paper for collecting radon progeny after their passing through the combination of wire screens, was introduced to compensate for the discrepancies (Fig. 3). Denoting the collection efficiencies for a combination of wire screens as $\varepsilon_{\mathrm{wire}}$, the overall collection efficiency for the sampling system $\varepsilon_{\mathrm{system}}$ is expressed as

$$\varepsilon_{\mathrm{system}} = \varepsilon_{\mathrm{wire}} - k(1-\varepsilon_{\mathrm{wire}}), \tag{4}$$

where k is the k-factor mentioned before.

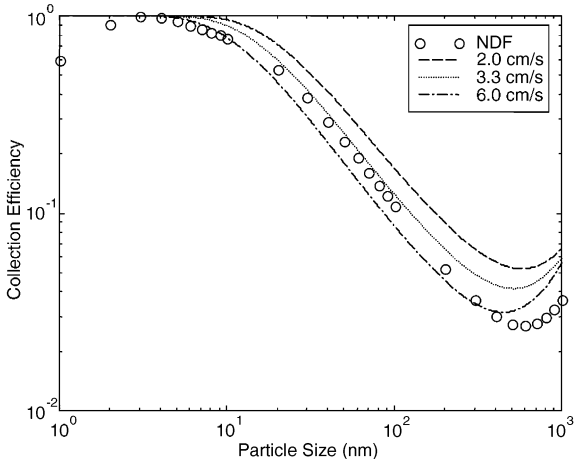

Fig. 1. The collection characteristics of four 400-mesh wire screens for various sampling face velocities U. The corresponding flow rate for 2.0, 3.3 and 6.0 cm s^{-1} were 1.5, 2.5 and 4.51 min^{-1}, respectively. Also shown is the calculated NDF value, for members of the public.

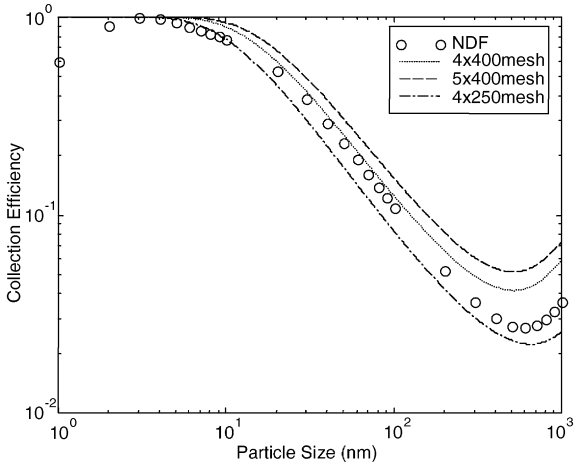

Fig. 2. The collection efficiencies of various series of wire screens at a sampling face velocity of 3.3 cm s^{-1}. Two types of wire screens were employed for purposes of comparison. Also shown is the value of NDF for members of the public.

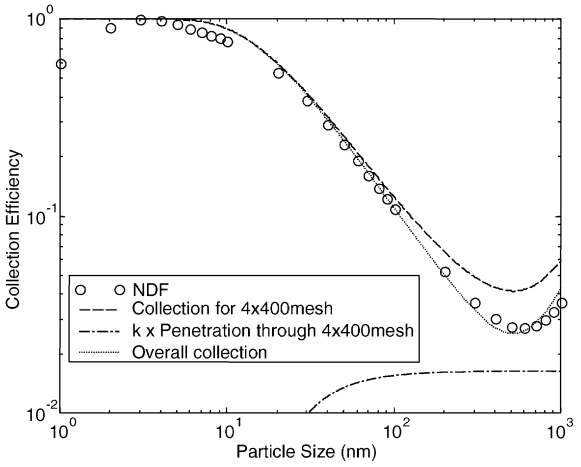

Fig. 3. The collection efficiency of the proposed sampling system, including the application of the k-factor. The sampling face velocity was 3.3 cm s^{-1} and the k-factor was 0.017. In fact, the penetration for 4×400-mesh was equivalently the collection on the filter paper. The NDF for members of the public with an n-factor of 2.66×10^{-4} mSv(s WL)$^{-1}$ is also shown.

2.3. Bronchial dosimeter

It is now possible to design a sampling system that can measure airborne radioactivity from which the DCC can

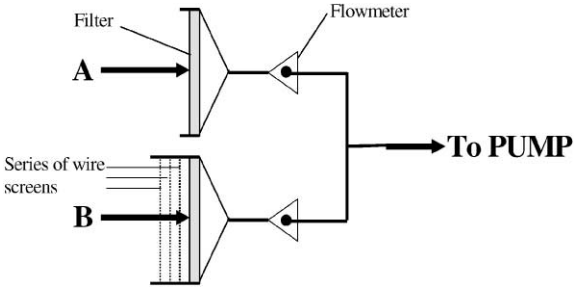

Fig. 4. Schematic diagram of the sampling system of the proposed radon progeny bronchial dosimeter. Two sampling heads are included. The choice of the wire-screen configuration in head B depends on the dosimetric lung model employed.

be estimated. The schematic diagram of such a sampler is shown in Fig. 4. It consists of two sampling heads, A and B. The sample head A houses only one filter paper and collects all radon progeny passing through it. Sample head B houses a series of stainless steel wire screens on top of a filter paper. The combination of the screen series is chosen according to the dosimetric lung model being used. For example, four 400-mesh screens with a sampling face velocity of $3.3\,\mathrm{cm\,s^{-1}}$ has been selected to simulate the NDF distribution curve for domestic exposures. The collected activities on both filter papers are measured using either gross alpha or alpha spectroscopic systems. Details of the required measurement techniques have been presented elsewhere (Yu et al., 1998). The collection efficiency of the wire screen series $\varepsilon_{\mathrm{wire}}$ is obtained by:

$$\varepsilon_{\mathrm{wire}} = \frac{\mathrm{PAEC_A\text{-}PAEC_B}}{\mathrm{PAEC_A}}, \tag{5}$$

where $\mathrm{PAEC_A}$ and $\mathrm{PAEC_B}$ are the measured PAECs collected on the filter papers in the sampling heads A and B, respectively. By using Eq. (4), the collection efficiency for the proposed system $\varepsilon_{\mathrm{system}}$ can be determined based on $\varepsilon_{\mathrm{wire}}$ and a selected value of k. The PAEC collected by the proposed system is computed by the product of $\varepsilon_{\mathrm{system}}$ and $\mathrm{PAEC_A}$. This is an integral count which effectively considers size distribution over the entire size range. When $\varepsilon_{\mathrm{system}}$ fits satisfactorily to the NDF distribution curve, the DCC is obtained by multiplying the calculated PAEC with the normalizing factor.

3. Results and discussion

The functional form of DCF against particle size has been determined in accord with the human respiratory tract model as proposed by ICRP (1994). The DCF, and thus EDF and NDF, has a strong dependence on particle size (Fig. 5). The largest NDF was obtained for

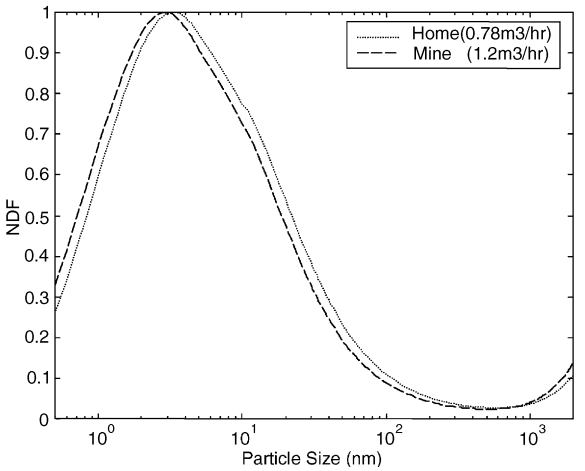

Fig. 5. Normalized effective dose rate (NDF) as a function of particle diameter for members of the public (Domestic home environment) and for mine workers (mine environment). The bracketed values represent the corresponding breathing rates for these two groups. The normalizing factors (n-factors) are 2.66×10^{-4} and $3.82\times10^{-4}\,\mathrm{mSv(s\,WL)^{-1}}$, respectively.

radon progeny with diameters of a few nm, corresponding to the unattached fraction. The NDF then decreases until about 300 nm due to decreasing diffusional deposition. Subsequently, it is observed to increase slightly due to the enhanced impactional and sedimental depositions for larger particles. The values for attached radon progeny are only 10–20% of those for the attached progeny. The calculated results for members of the public and for mine workers have also been compared as shown in Fig. 5, which is effectively a comparison of breathing rates; higher breathing rates lead to an increase in the deposition of radon progeny. Also, the maximum NDF value is shifted to a lower particle diameter for larger breathing rates, as applicable in mine working conditions. It is to be noted that the n-factors for the two groups are different, the maximum values of both NDF distributions being normalized to unity. For domestic exposures, the n-factor is $2.66\times10^{-4}\,\mathrm{mSv(s\,WL)^{-1}}$, transforming to an effective dose rate of $2.66\times10^{-4}\,\mathrm{mSv\,s^{-1}}$ for a nominal PAEC of 1 WL. For mine exposures, the n-factor is $3.82\times10^{-4}\,\mathrm{mSv(s\,WL)^{-1}}$, which transforms to an effective dose rate of $3.82\times10^{-4}\,\mathrm{mSv\,s^{-1}}$ for 1 WL, which is higher than the corresponding value for the general public.

The functional forms of the NDF distribution curves for both groups have been simulated using various combinations of wire screens in series and using different sampling face velocities (corresponding to different sampling flow rates). Two types of wire screen, with different mesh numbers, were employed. Both were stainless steel metal wire screens with a specific density

Table 1
Summary of the measured parameters for the wire screens employed

Mesh number	Screen diameter (cm)	Mass of screen (g)	Screen thickness (μm)	Wire diameter (μm)
250	4	0.2328	87.5	37
400	4	0.1929	57	27.5

of 7.8 g cm^{-3}. Other measured parameters are summarized in Table 1. The fits to the NDF profiles are shown in Figs. 1 and 2. Since the sampled volume is a critical factor, affecting counting statistics, the sampling flow rate should not be too small. In practice, a practical flow rate was assumed at the beginning. Various multiple wire screens in series were then tested in efforts to obtain a fit to the NDF curve. On identifying the combination with the best fit, different sampling flow rates were applied to this wire screen configuration. An increase in the flow rate in general led to a shift of the collection efficiency towards smaller particle sizes. It should also be noted that a larger sampling flow rate or face velocity will cause a decrease in the diffusion deposition of radon progeny onto the wire screen. Again, the flow rate with the best fit was ascertained. In this way, the best combination of wire screens as well as the best flow rate could be specified. Thus said, in reality, similar fits could be obtained using different wire screen configurations and flow rates. The following discussion will be restricted to the use of four 400-mesh wire screens with sampling face velocities of 3.3 and 4.6 cm s^{-1} for domestic and mine exposures, respectively.

The attached fraction of PAEC is described by a log-normal distribution, with an activity median diameter (AMD) of 200 nm for domestic conditions and 250 nm for mine conditions (Zock et al., 1996). The geometric standard deviation (GSD) was defined by the ICRP formula (ICRP, 1994). For these values, the analysis for the attached mode was restricted to particle sizes ranging from 50 nm to 1000 nm. The abundance at these two size limits drops to less than one-third of the maximum value.

The discrepancies between the collection efficiencies and the NDF values can be substantial at large particle sizes, ranging from several tens of nm up to μm-sized particles. This range corresponds to the attached fraction of radon progeny, which is the major portion (over 90%) of the total PAEC of progeny in almost all environmental situations (NRC, 1991). Accordingly, the unattached fraction of PAEC for underground mines only contributes to less than 8% of the DCC (Birchall and James, 1994). Hence, the uncertainty due to the sampler system which simulates the NDF curve can be greatly minimized once the region of the attached mode is associated with a satisfactory fit.

In the present study, a k-factor has been introduced in an attempt to improve the fit which characterizes the attached mode. Here, the penetration through the wire-screen series is multiplied by the k-factor, which is to be subtracted from the collection efficiencies of the wire-screen series. The reduced collection efficiencies give a much better match to the NDF values for the attached mode (Fig. 3). The value of the k-factor was determined by minimizing the χ^2 values computed at particle sizes from 50 nm up to 100 nm, with steps of 10 nm, and at particle sizes above 100 nm, with steps of 50 nm. Before the application of the k-factor, the discrepancy between the calculated DCC value and the actual value for attached mode was found to be in excess of 12% for typical domestic conditions and nearly 20% for typical mine conditions; the gross error in the final DCC value was greater than 20% for both conditions. On introducing the k-factor, the error contributed by the attached mode became less than 1% for typical domestic conditions, and the gross error in the final DCC value was reduced to around 10%; the corresponding values for typical mine conditions were below 1% and approximately 2.5%, respectively.

For domestic exposures, the best configuration was the use of four 400-mesh wire screens for a sampling flow rate of 2.5 l min^{-1} or equivalently a sampling face velocity of 3.3 cm s^{-1}. Close matches to the NDF pattern could also be achieved by various wire-screen systems, such as five 400-mesh wire screens with a sampling face velocity of 4.6 cm s^{-1} or three 400-mesh wire screens with sampling face velocity of 2 cm s^{-1}. Even with the same sampling flow rate of 2.5 l min^{-1}, the configuration with six 250-mesh wire screens demonstrated a good fit. The possible wire-screen systems for fitting the NDF pattern are presented in Table 2. For mine conditions, four 400-mesh wire screens with sampling face velocity of 4.6 cm s^{-1}, five 400-mesh screens with 5.3 cm s^{-1}, and three 400-mesh screens with 2.7 cm s^{-1} were capable of providing adequate match to the NDF curve. The results are also summarized in Table 2.

In the previous discussion, the collection efficiency of the proposed sampling system was always equal to unity for particle sizes below 3 nm, also apparently overestimating the NDF distribution. However, as discussed before, the contribution from the unattached progeny (with diameters between 0.5 and 5 nm) to the final DCC is less important compared to that from the attached

Table 2
Summary of possible wire-screen systems providing good fits to the predicted NDF distribution. Negative values in the estimated error represent underestimation while positive values represent overestimation. The wire parameters for the wire screens employed can be found in Table 1

Exposure condition	Wire-screen system	Sampling flow rate ($l\,min^{-1}$)	k-factor	Estimated error to DCC from the attached mode (bracketed values are error estimates without taking the k-factor into account)
Domestic homes	4×400-mesh	2.5	0.017	0.12% (12.4%)
	6×250-mesh	2.5	0.010	1.45% (8.7%)
	5×400-mesh	3.5	0.020	−0.77% (13.7%)
	5×400-mesh	3.0	0.025	2.29% (20.2%)
	3×400-mesh	1.5	0.014	4.27% (14.4%)
Mine	4×400-mesh	3.5	0.013	0.38% (19.3%)
	5×400-mesh	4.0	0.022	2.93% (34.6%)
	3×400-mesh	2.0	0.011	7.02% (23.0%)

mode. Taking into account the unattached fraction of PAEC of 8% and 1% in homes and mines, respectively, the error from this mode is around 10% for homes and around 2% for mines. The discrepancies between the collection efficiency and the NDF distribution within this region was therefore neglected in the previous discussion.

The discrepancies can be reduced through measurements made with an additional single 100-mesh wire screen (with wire diameter of 112 μm, screen thickness of 215 μm and solid volume fraction of 0.313) (Solomon, 1997) and with a sampling face velocity of $3.3\,cm\,s^{-1}$ (applicable for the discussions of the four 400-mesh wire-screen configurations with a sampling face velocity of $3.3\,cm\,s^{-1}$ for domestic exposures). To remedy the overestimation mentioned in the preceding paragraph, the collection efficiency of this 100-mesh wire screen (ε_{100}) was determined, multiplied by a factor f as presented in Fig. 6, and then subtracted from the collection efficiency of the four 400-mesh wire screens (ε_{400}). A new n-factor for the NDF is required in order to provide a satisfactory match with the resulting collection efficiency. Again, the k-factor is adopted to obtain the best fit to the attached region by minimizing the corresponding χ^2 value. With this, the overall collection efficiency of the system becomes

$$\varepsilon_{system} = \varepsilon_{400} - k(1-\varepsilon_{400}) - f\,\varepsilon_{100}, \quad (6)$$

with $k = 0.018$, $f = 0.4$ and an n-factor $= 2.39\times10^{-4}\,mSv(s\,WL)^{-1}$. The errors of the calculated DCC are then found to decrease from 16% to 1% for the unattached mode and from over 20% to less than 4% for the attached mode.

In practice, the filter paper housed in the sampling head A in the original sampling system is now covered with an additional 100-mesh wire screen. For this configuration, the PAEC collected on the 100-mesh screen is required to be measured directly as $PAEC_{100}$. The total

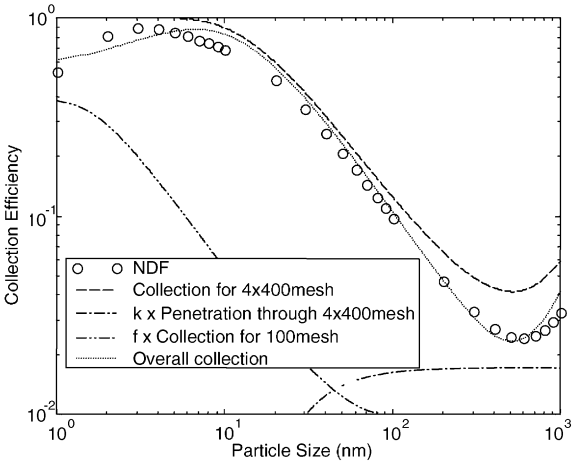

Fig. 6. The collection efficiency of the proposed sampling system. The discrepancies in the unattached mode is diminished through measurements employing an extra 100-mesh wire screen while discrepancies in the attached mode are corrected by the k-factor. The sampling face velocity is $3.3\,cm\,s^{-1}$, the k-factor is 0.018, while f is equal to 0.4. The NDF for members of the public with n-factor of $2.39\times10^{-4}\,mSv(s\,WL)^{-1}$ is also shown.

PAEC in air $PAEC_T$ and the collection efficiencies of the wire screen, ε_{100} and ε_{400} are calculated as:

$$PAEC_T = PAEC_{100} + PAEC_A, \quad (7)$$

$$\varepsilon_{100} = \frac{PAEC_{100}}{PAEC_T}, \quad (8)$$

$$\varepsilon_{400} = \frac{PAEC_T - PAEC_B}{PAEC_T}, \quad (9)$$

where $PAEC_A$ and $PAEC_B$ are the PAEC values recorded by the filter papers housed in sampling heads

A and B, respectively. The DCC is computed by multiplying the calculated PAEC for the overall system and the n-factor.

4. Conclusions

The design of a bronchial dosimeter which gives the bronchial dose from radon progeny by direct measurements has been proposed in this paper. The prime advantage of this dosimeter is that no requirement exists for the measurement of the size distribution of radon progeny. Additional assumptions on calculations are not required after measurements.

The particle size dependence of the NDF, which is normalized from the dose conversion factor, can be simulated by the collection efficiency of the proposed wire-screen sampling systems. In the present work, we further aim to minimize discrepancies due to simulation in the particle size region corresponding to the attached mode of radon progeny, with the contribution from the attached mode towards the DCC being the major portion. Thus, a so-called k-factor has been introduced, leading to a satisfactory fit in the attached-mode region. Various combinations of wire-screens in series have been found capable of providing satisfactory fits to the NDF pattern. A four 400-mesh wire-screen configuration provided best fits for both domestic and mine exposures, with sampling flow rates of 2.5 and 3.51 min^{-1}, respectively. After applying the k-factor, the estimated errors for the sampling systems in the DCC contributed by the attached mode decreased from over 12% to less than 1%. The values of k-factor were obtained as 0.017 and 0.013 for home and mine conditions, respectively.

In the previous studies, a pre-separator has been suggested for cutting out a part of the unattached radon progeny, allowing a good fit for the unattached-mode region of the NDF response (Solomon, 1997). However, this pre-separator would screen out most of the unattached fraction of PAEC in air, with the resulting alpha counts on the succeeding wire screen being very small. In the present paper, an alternative method, providing a good fit in the unattached-mode region has been introduced. This required an extra 100-mesh wire screen and a measurement of the PAEC was recorded on this screen. With this, the overall error in the DCC reduces to around 3%.

Uncertainties in the development of dosimetric lung models remain while dose conversion coefficients are yet to be changed. However, the proposed sampling system (configuration and sampling face velocity) can easily be modified to suit the updated dosimetric lung models. The k-factor can always be used as a fine-tuning technique.

Acknowledgements

This research was supported by a research grant 7001101 from the City University of Hong Kong.

References

Birchall, A., James, A.C., 1994. Uncertainty analysis of the effective dose per unit exposure from radon progeny and implications for ICRP risk-weighting factors. Radiat. Prot. Dosim. 53, 133–140.

Cheng, A.Y.S., Yeh, H.C., 1980. Theory of screen type diffusion battery. J. Aerosol Sci. 11, 313–319.

Cheng, A.Y.S., Keating, J.A., Kanapilly, G.M., 1980. Theory and calibration of a screen-type diffusion battery. J. Aerosol Sci. 11, 549–556.

Hopke, P.K., Ramamurthi, M., Knutson, E.O., 1990. A measurement system for radon decay product lung deposition based on respiratory models. Health Phys. 58, 291–295.

ICRP, International Commission on Radiological Protection, 1994. Human respiratory tract model for radiological protection. ICRP Publication 66. Pergamon Press, Oxford.

James, A.C., 1984. Dosimetric approaches to risk assessment for indoor exposure to radon daughters. Radiat. Prot. Dosim. 7, 353–366.

James, A.C., Stahlhofen, W., Rudolf, G., Egan, M.J., Nixon, W., Gehr, P., Briant, J.K., 1991. The respiratory tract deposition model proposed by the ICRP Task Group. Radiat. Prot. Dosim. 38, 159–165.

NRC, National Research Council, 1991. Comparative dosimetry of radon in mines and homes. National Academic Press, Washington, DC.

Oberstedt, S., Vanmarcke, H., 1995. The bronchial dosemeter. Radiat. Prot. Dosim. 59, 285–290.

Porstendörfer, J., 1996. Radon: measurements related to dose. Environ. Inter. 22, S564–S583.

Ramamurthi, M., Hopke, P.K., 1989. On improving the validity of wire screen unattached fraction Rn daughter measurements. Health Phys. 56, 189–194.

Solomon, S.B., 1997. A radon progeny sampler for the determination of effective dose. Radiat. Prot. Dosim. 72, 31–42.

Yu, K.N., Guan, Z.J., Young, E.C.M., Stokes, M.J., 1998. Measurement of tracheobronchial dose from simultaneous exposure to environmental radon and thoron progenies. Health Phys. 75, 153–158.

Zock, C., Porstendörfer, J., Reineking, A., 1996. The influence of biological and aerosol parameters of inhaled short-lived radon decay products on human lung dose. Radiat. Prot. Dosim. 63, 197–206.